The onset of sediment transport in vegetated channels predicted by turbulent kinetic energy

J. Q. Yang [1]*, H. Chung [1], and H. M. Nepf [1]

[1]Department of Civil and Environmental Engineering, Massachusetts Institute of Technology, Cambridge, Massachusetts, USA

Key Points:

- The critical velocity for sediment motion decreases with increasing vegetation density
- Near-bed turbulent kinetic energy describes the critical condition for sediment motion for both bare and vegetated channels
- A model for critical velocity based on near-bed turbulence unifies bare-bed and vegetated channel conditions

*Current address,15 Vassar Street, Cambridge, Massachusetts

Corresponding author: J. Q. Yang, qjyang@mit.edu

Abstract

This laboratory study advances our understanding of sediment transport in vegetated regions, by describing the impact of stem density on the critical velocity, U_{crit}, at which sediment motion is initiated. Sparse emergent vegetation was modeled with rigid cylinders arranged in staggered arrays of different stem densities. The sediment transport rate, Q_s, was measured over a range of current speeds using digital imaging, and the critical velocity was selected as the conditions at which the magnitude of Q_s crossed the noise threshold. For both grain sizes considered here (0.6-0.85mm and 1.7-2mm), U_{crit} decreased with increasing stem density. This dependence can be explained by a threshold condition based on turbulent kinetic energy, k_t, suggesting that near-bed turbulence intensity may be a more important control than bed shear stress on the initiation of sediment motion. The turbulent kinetic energy model unified the bare-bed and vegetated channel measurements.

1 Introduction

Aquatic vegetation provides important ecosystem services [e.g. *Micheli and Kirchner*, 2002; *Kremen*, 2005; *Danielsen et al.*, 2005], whose global value has been estimated to be in the tens of trillion dollars per year [*Costanza et al.*, 1997]. However, a large amount of aquatic vegetation has been lost in recent decades, including over half of the wetlands and thousands of acres of seagrass in the U.S [*Marani et al.*, 2011]. An understanding of sediment transport in vegetated regions is essential for vegetation restoration because the evolution of vegetated landscape occurs through the interplay of flow, vegetation and sediment accretion. Yet, there are currently no predictive models for sediment transport in vegetation. This study takes a first step toward developing a sediment transport model by quantifying the incipient conditions for sediment transport in vegetated regions.

In a bare channel the critical velocity defining incipient sediment motion, U_{crit}, has historically been related to the time-mean bed shear stress (τ) [*Shields*, 1936]. However, more recent studies support the role of turbulence in initiating sediment motion [*Heathershaw and Thorne*, 1985; *Nelson et al.*, 1995; *Diplas et al.*, 2008]. In a bare channel, the role of turbulence may be inherently represented in the Shields diagram because the turbulent kinetic energy and τ are linearly related [*Stapleton and Huntley*, 1995]. In a vegetated channel, however, the turbulence is predominantly generated by the vegetation [*Tanino and Nepf*, 2008a; *Stoesser et al.*, 2010], such that τ is no longer a surrogate for near-bed turbulence. This may explain why bed shear stress models based on open channel studies do

not work in vegetated channels [*Yager and Schmeeckle*, 2013; *Hongwu et al.*, 2013; *Tinoco and Coco*, 2014].

In this paper, we assume that the near-bed turbulence plays the central role in initiating sediment motion, as also proposed by *Nelson et al.* [1995] and *Diplas et al.* [2008]. A prediction for U_{crit} is devised based on the near-bed turbulence generated by both bed shear stress and vegetation wakes. The model is shown to be consistent with measurements made in bare and sparsely vegetated channels.

2 Theory

Previous studies have shown that the initiation of grain motion is connected to the passage of turbulent eddies and the associated fluctuations in near-bed pressure, which generate sufficient instantaneous lift and drag forces to destabilize the grains [*Smart and Habersack*, 2007; *Zanke*, 2003]. Because the magnitude of the fluctuating drag and lift forces are correlated with the near-bed turbulent kinetic energy (k_t), we propose using k_t as a predictor of the incipient condition of sediment transport. This proposal is supported by observations of sediment erosion over a bare bed and a bed with *Spartina anglica* at different stem densities [*Widdows et al.*, 2008]. In the Widdows study, the relation for open channel flow, $\tau = 0.19k_t$, was used to estimate the mean bed stress from the measured turbulent kinetic energy $k_t = (\overline{u'^2} + \overline{v'^2} + \overline{w'^2})/2$, with u', v', w' denoting the velocity fluctuation [*Stapleton and Huntley*, 1995]. However, as discussed in [*Nepf*, 2012a; *Ricardo et al.*, 2014; *Yang et al.*, 2015], this relation assumes turbulence production is linked to bed stress, which is not true in vegetated systems, for which turbulence production is primarily associated with the vegetation. Therefore, Widdows' conclusion that the critical τ was unchanged between bare and vegetated beds (Figure 6 in [*Widdows et al.*, 2008]) was incorrect, and in fact their data actually shows that the threshold for erosion was defined by a critical value of k_t. Finally, the duration of the turbulence-driven lift and drag is also important, and may be characterized by an impulse parameter [e.g. *Celik et al.*, 2010, 2013]. The duration is connected to eddy scale, which in turn is connected to the grain size and stem diameter, so that for a fixed grain size and stem diameter, k_t alone should set the critical threshold.

Over a bare channel, the near bed k_t is proportional to τ [*Stapleton and Huntley*, 1995], and τ is proportional to the time-mean, depth-average velocity squared U^2 [*Wilcock*,

1996; *Julien*, 2010]. Specifically, $k_{tb} = C_b U^2$, with C_b a coefficient dependent on the bed roughness. In a vegetated channel, both the bed-generated turbulence and the vegetation-generated turbulence contribute to the near bed k_t. For simplicity, we assume that the total near-bed k_t is the sum of the two, neglecting any mutual influence. For a sparse emergent canopy, specifically $d/s_n < 0.56$ with d and s_n denoting the stem diameter and the average surface-to-surface distance between the nearest stem neighbor, respectively, which we consider in this study, stem-scale eddies can exist throughout the canopy, so that the vegetation-generated turbulence can be described by equation (4.1) in [*Tanino and Nepf*, 2008a]:

$$k_{tv} = 1.2[C_D \frac{\phi}{(1-\phi)\pi/2}]^{2/3} U^2. \tag{1}$$

Here C_D is the stem drag coefficient and ϕ is the solid volume fraction within the canopy. In order for equation (1) to apply, the stem Reynolds number Re_d ($= Ud/\nu$) must be larger than 120 for stem wake turbulence to be generated [*Liu and Nepf*, 2016]. In this study $600 < Re_d < 2500$ and $d/s_n \leq 0.25$ ($\phi \leq 5\%$), so that $k_{tv} \approx 1.2(\frac{C_D \phi}{\pi/2})^{2/3} U^2 \approx 0.9 C_D^{2/3} \phi^{2/3} U^2$. Assuming that the total near-bed k_t is the sum of k_{tb} and k_{tv}, the total near bed k_t in a sparse emergent canopy can be estimated as:

$$k_t = C_b U^2 + 0.9 C_D^{2/3} \phi^{2/3} U^2. \tag{2}$$

If k_t sets the threshold for incipient sediment motion, then equation (2) can be used to predict the critical velocity. The critical k_t should be a function of the sediment size (d_s). For vegetated and bare channels with the same d_s, $C_b U_{crit}^2 + 0.9 C_D^{2/3} \phi^{2/3} U_{crit}^2 = C_b U_o^2$, with U_o denoting the critical velocity for a bare bed, i.e. $U_{crit} = U_o$ when $\phi = 0$. Re-arranging,

$$\frac{U_{crit}}{U_o} = \frac{1}{\sqrt{1 + C\phi^{2/3}}}. \tag{3}$$

in which the coefficient $C = 0.9 C_D^{2/3} / C_b$. Estimations of C_b and C_D can be found in [*Julien*, 2010] and [*Tanino and Nepf*, 2008b; *Cheng and Nguyen*, 2011], respectively. Hereafter equation (3) is referred to as the turbulence model for sparse vegetation. For dense vegetation ($d/s_n \geq 0.56$), the turbulence generated in the stem wakes has a weaker dependence on solid volume fraction [Figure 14 and equation (4.1) in *Tanino and Nepf*, 2008a], so that U_{crit} is expected to have a weaker dependence on ϕ compared with the sparse vegetation (equation (3)).

3 Methods

The model emergent vegetation was created using rigid circular cylinders with diameter $d = 6.3mm$ fixed in a staggered pattern in PVC boards (Figure 1). The solid volume fraction (ϕ) ranged from 0.006 to 0.05, similar to conditions found in marshes [*Nepf*, 2012b]. One layer of sieved light-brown sand was glued to the PVC boards. Two sand sizes (d_s) were used: 0.6 to 0.85mm and 1.7 to 2mm. The boards were placed in a horizontal recirculating flume with a 1-m wide and 10-m long test section. Flow was generated by a centrifugal pump and measured with an in-line flow meter with $0.001m^3/hr$ precision. The measured flow rate, Q, was used to estimate the average channel velocity $U = Q/(wh(1-\phi))$, with w and h denoting channel width and water depth, respectively. A digital camera was placed approximately 1m downstream from the leading edge of the boards to observe the sand motion (Figure 1b). h was measured close to the camera and was controlled to be 20 to 22cm.

A layer of black sand with the same size distribution as the light-brown sand was spread on top of the light-brown sand. The motion of the black sand was recorded at 60 frames per second with a 1280×960-pixels camera and a 35mm fixed focal length lens (Figure 1b). The original imaging area was around 10cm by 7.6cm with one grain diameter corresponding to 10 to 20 pixels. To capture the spatial heterogeneity of sediment motion, the imaging window contained an integral number of the repeated pattern of dowels (Figure 1a). To eliminate distortions in the image due to water surface movement, a small glass tank was positioned above the channel and extended less than 1 cm below the water surface (Figure 1c).

The following steps were used to estimate the sand transport rate, Q_s. First, in each frame the percentage of the pixels occupied by black sand grains was defined as the black sand occupancy, P_{blk}. Second, the trajectory of each black grain (Figure 1a) was identified using IDL particle tracking MatLab code written by *Crocker and Grier* [1996]. Third, the average streamwise velocity of the black sand grains (U_p) was calculated from the identified trajectories, producing an average velocity for all particles over 30 seconds. The volume of particles in motion per unit bed area (γ) was estimated from the number of moving particles averaged over the 1800 frames. The black sand transport rate was then calculated as $Q_{blk} = U_p\gamma$ [*Wong et al.*, 2007; *Furbish et al.*, 2012]. Assuming sand motion only occured in the top layer [*Houssais et al.*, 2015] and all sand motion followed the

same probability distribution, the total sediment transport rate Q_s for a full bed of loose grains can be estimated as $Q_s = Q_{blk}/P_{blk}$. We calculated Q_s for different imaging durations and found that Q_s converged to a constant value at less than 30 seconds.

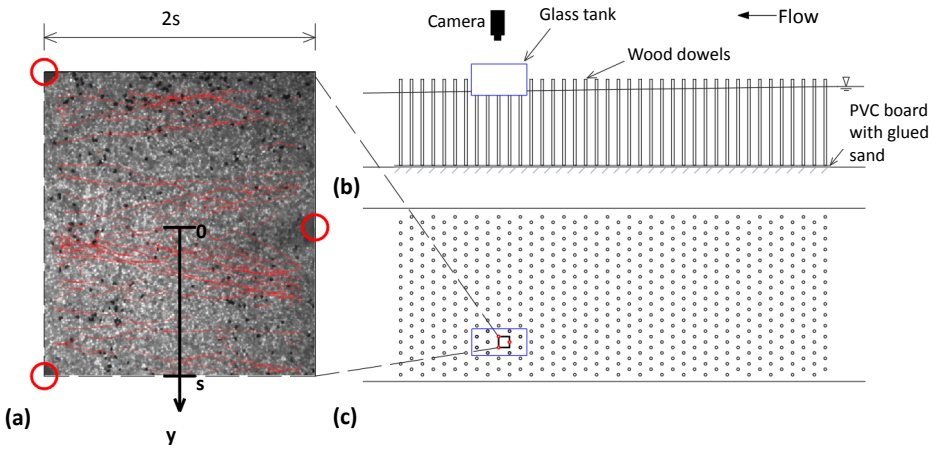

Figure 1. (a)The gray-scale image of the sand bed with superimposed trajectories of moving black sand (the red lines). The flow was right to left in the image. The red circles indicate the positions of dowels. LDV measurements were taken along the y axis defined, as shown in (a), at the mid-point of the unit cell of the repeating dowel pattern. $y = 0$ (the center of the image) was in line with the upstream dowel and mid-way between the upstream and downstream dowel rows. $y = s$ (lower edge of the image) was in line with the downstream dowel. (b) Side view of the test section. Vertical circular cylinders represent emergent stems of vegetation. The digital camera, with polarizing lens, was positioned above a glass tank with 15cm width and 30cm length in the horizontal plane. Several dowels under the tank were cut to allow the bottom of the tank to touch the water surface. (c) Top view of the test section shown in (b). The dowels were placed in a staggered pattern. The black box with red circles inside the blue box (the glass tank) represents the region captured by the camera.

For each vegetation solid volume fraction (ϕ) the sediment transport rate (Q_s) was measured at several channel velocities (U). A reference video with no black sand was also recorded for each flow condition and used to define the noise level. For each sediment size, the maximum noise value was used as the threshold criterion for sediment motion, Q_{s-crit}. For each vegetation density, an upper and lower bound for U_{crit} was chosen such that above the upper bound all the measured Q_s were larger than Q_{s-crit} and below the

lower bound all the measured Q_s were smaller than Q_{s-crit}. The mean between the upper and lower bound was chosen as U_{crit}.

The instantaneous velocity (u, w) was recorded at the critical condition ($U = U_{crit}$) using backscatter Laser Doppler velocimetry (LDV) at 1mm above the bed. Here (u, v, w) refer to the velocity along the x, y, z axes, corresponding to the steamwise, spanwise and vertical directions, respectively. The distance to the bed (1mm) was chosen to characterize the near bed flow condition because the fluid structures that trigger particle motion scale with sediment size [*Vowinckel et al.*, 2016]. The LDV probe (Dantec Dynamics) was mounted on a manually-driven positioning system, and the velocity was measured above the bed area where the sediment transport videos were recorded. For each velocity record, 10000 samples were collected at frequencies from 5 to 100 Hz. For the majority of the measurements, the sampling frequency was greater than twice the integral time scale from the autocorrelation function [*Nezu et al.*, 1994; *Kundu et al.*, 2008], indicating that the sampling frequency was sufficient to capture the characteristics of the turbulence. The running average of turbulent statistics (including Reynolds stress and k_t) converged to stable values within 10000 velocity samples, consistent with a previous study [*Buffin-Bélanger and Roy*, 2005].

Because the 2-D LDV only measured the vertical (w) and streamwise (u) velocity the turbulent kinetic energy was approximated as $k_t = (2\overline{u'^2} + \overline{w'^2})/2$. This approximation is justified because previous measurements have shown that within an emergent array the kinetic energy contributed by span-wise velocity fluctuation ($\overline{v'^2}$) is approximately equal to ($\overline{u'^2}$) [*Tanino and Nepf*, 2007]. For the vegetated cases, velocity was recorded along a lateral transect midway between rows at y/s = 0, 0.25, 0.5, 0.75 and 1, where s is the distance between dowels defined in Figure 1a. For the bare bed, the velocity was measured at two positions located laterally 5cm apart.

To show that the selected lateral positions captured the flow heterogeneity and provided representative spatial averages, we also measured the velocity for 3 minutes each at 18 vertical locations at the selected lateral positions. The average channel velocity estimated from these vertical profiles agreed with the flow meter reading within 10%, indicating that our selected lateral positions were adequate to characterize the flow heterogeneity. Furthermore, the LES results shown in figure (10) of [*Stoesser et al.*, 2010] confirm that for sparse vegetation our lateral transect captured most of the flow heterogeneity.

4 Results

Above a critical channel velocity, the sediment transport rate Q_s increased steadily with increasing U (Figure 2). The black dashed line denotes the noise threshold, $Q_{s-crit} = 0.01mm^2/s$. Once sediment transport was initiated, the sediment transport rate was consistently higher for cases with model vegetation, compared to bare-bed, and at the same channel velocity the sediment transport rate generally increased with increasing vegetation solid volume fraction (ϕ).

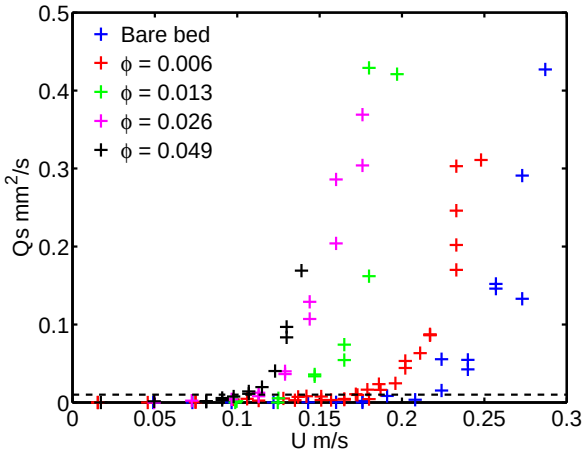

Figure 2. Sediment transport rate, Q_s, versus channel velocity, U, for bare bed and four vegetation solid volume fractions (ϕ). The sediment size d_s = 0.6 to 0.85mm. The horizontal dashed line denotes the critical sediment transport rate, $Q_{s-crit} = 0.01mm^2/s$ defined based on the noise threshold.

The incipient velocity (U_{crit}) was identified from the Q_s and U data as described in the Methods section. For both grain sizes the value of U_{crit} decreased with increasing vegetation solid volume fraction (ϕ), with the greatest drop between the bare bed and the sparsest stem density (Figure 3). As expected, the values of U_{crit} were higher for the larger grain size. *Hongwu et al.* [2013] estimated similar values of U_{crit} as a function of stem density for a grain size comparable to our smaller grain (data included in Figure 3).

The spatially-averaged near-bed turbulence, k_t, was measured at the critical condition ($U = U_{crit}$) for each stem density (red symbols in Figure 4). To clarify overlapping points, the $x-$axis of measured k_t has been shifted right by 0.001. The lower and upper bound of measured k_t correspond to the value of k_t measured at U equal to the lower and upper bound of U_{crit}, respectively. Note that the spatial heterogeneity of k_t is much

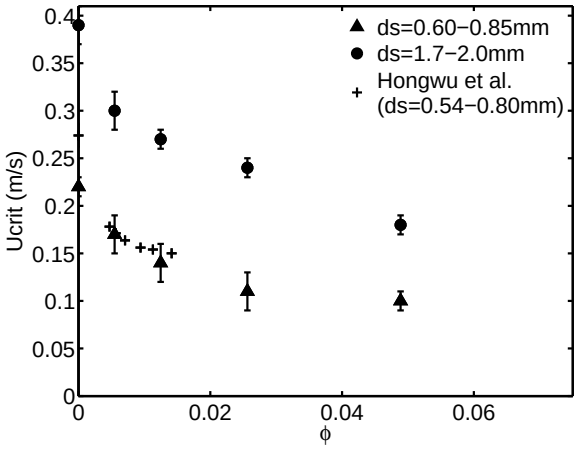

Figure 3. The critical velocity for sediment motion, U_{crit}, versus vegetation solid volume fraction, ϕ. The filled triangles and circles with error bars are from the present study. The crosses are from [*Hongwu et al.*, 2013] .

smaller than the error of k_t due to the uncertainty in U_{crit}. Within uncertainty the critical k_t was constant across all stem densities and bare bed.

To further support the turbulence model, the near-bed turbulence was also estimated using equation (2). The bed turbulence coefficient, C_b, was estimated from the measured bare-bed values of $k_t = 0.0012m^2/s^2$ and $U_o = 0.22m/s$, specifically $C_b = k_t/{U_o}^2 = 0.025$. Previous bare-bed studies have shown that the near-bed $k_t \approx 5.3\tau/\rho$ [*Stapleton and Huntley*, 1995] and $\tau/\rho = C_f U^2$ [*Wilcock*, 1996]. For the conditions in this study ($h \approx 0.2m, d_s = 0.6 - 0.85mm$) $C_f \approx 0.0034$ (the Darcy-Weisbach friction relation in [*Julien*, 2010]), from which a predicted C_b is 0.02, agreeing with the measure value (0.025) within 25%. The value for C_D was approximated as 1.0 ± 0.5 for our experimental conditions ($600 < Re_d < 2500$) based on experimental data compiled in [Figure 4, *Cheng and Nguyen*, 2011]. As ϕ increased, the contribution from the bed-generated turbulence k_{tb} (black squares in Figure 4) decreased significantly due to the decrease of U_{crit}. In contrast, the estimated contribution from vegetation-generated turbulence k_{tv} (black diamonds in Figure 4) increased with increasing ϕ because increasing the stem density provided more site for stem-wake turbulence generation (equation (1)). The predicted $k_{tb}+k_{tv}$ (equation (2), or the black circles) agreed with the measured k_t (the red symbols) within uncertainty, which both validated equation (2) and supported the hypothesis that the critical velocity was set by a threshold in near-bed k_t.

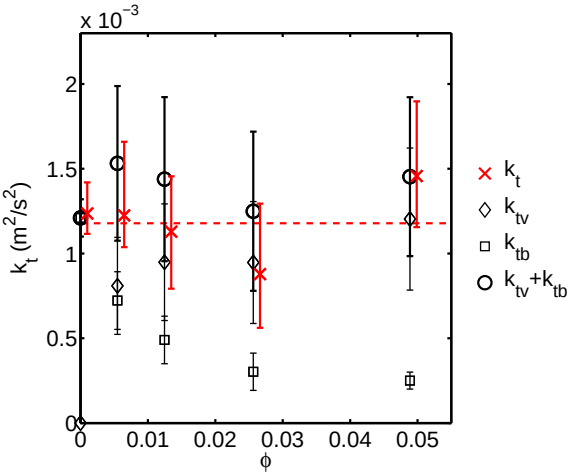

Figure 4. The measured turbulent kinetic energy (k_t, red symbols) and the predicted contribution from bed-generated turbulence k_{tb} and vegetation-generated turbulence k_{tv} at the critical condition ($U = U_{crit}$) for d_s = 0.6-0.85mm. The horizontal dashed line represents the average of measured k_t weighted by 1 over the error of k_t. The errors in k_{tb} and k_{tv} were contributed by the uncertainty in U_{crit} and C_D through standard propagation of error [e.g. *Taylor*, 1997]. For k_{tv}, the uncertainty in C_D contributed to the majority of its error.

In Figure 5, the measured U_{crit}, normalized by the critical velocity for bare bed, U_o, is compared to the turbulence model described by equation (3). First, normalizing by U_o collapsed the two data sets (triangle and circles in Figure 5) within uncertainty, consistent with equation (3). Second, the model prediction with $C_b = 0.025$ and $C_D = 1$ is shown with a black dashed curve. The uncertainty in the predicted U_{crit}/U_o (gray shadow in Figure 5)) arose mainly from the uncertainty in $C_D(= 1 \pm 0.5)$. Both of our experimental data sets and the data from [*Hongwu et al.*, 2013] (plus signs) agree with the turbulence model within uncertainty.

The model also has good agreement with the measurements of *Widdows et al.* [2008] which use natural vegetation (*Spartina anglica*) and natural mud with median grain size around $17.4 \pm 0.2\mu m$ (diamonds in Figure 5). In their study, U_{crit} was defined as the velocity required to erode 10 grams of sediment per unit bed area, extrapolated from the suspended mass versus velocity curve. We estimated the solid volume fraction of *Spartina* (ϕ) as $\pi d^2 n/4$ with n denoting the number of stems per bed area, which is reported in the paper. *Spartina anglica* leaves are 1.5cm wide at the base and taper to a point, so that 0.75 cm was chosen as an estimation of d. The values of U_{crit}/U_o versus ϕ (diamonds

in Figure 5) agree with the turbulence model within uncertainty, indicating that the turbulence model can be extended to conditions with natural vegetation and fine sediment.

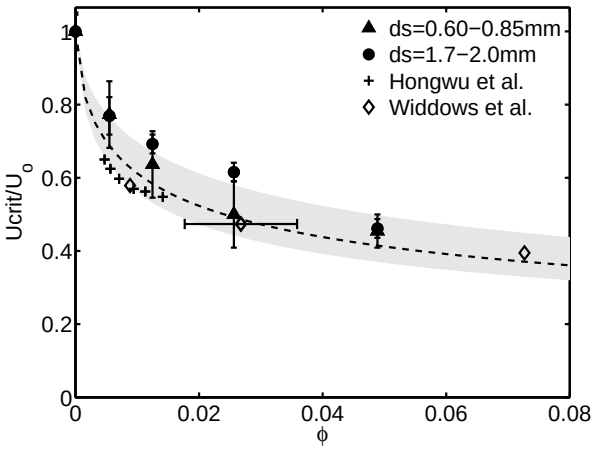

Figure 5. The incipient velocity of sediment motion U_{crit} normalized by the incipient velocity for a bare bed with the same sediment size (U_o). The black dashed curve with gray shadow represents the turbulence model (equation (3)) with $C_b = 0.025$ and $C_D = 1 \pm 0.5$. The black dashed curve corresponds to $C_D = 1$, and the upper and lower edge of the gray region represent $C_D = 0.5$ and 1.5, respectively. The horizontal bar for the diamond symbol at $\phi \approx 0.025$ represents the range of ϕ reported for this condition [*Widdows et al.*, 2008].

Finally, the difference between U_{crit} values measured with different grain sizes (Figure 3) is consistent with U_{crit} set by a critical value of k_t. As noted by previous researchers [e.g. *Smart and Habersack*, 2007], let's assume that the eddy-induced pressure fluctuations initiate sediment motion. From Bernoulli's equation, the eddy-induced pressure fluctuation P_e should scale as $\rho {U_e}^2$, with U_e denoting the eddy velocity. Because ${U_e}^2$ is proportional to k_t, P_e is proportional to k_t. Consider a grain of size d_s, at the critical condition the lift force on the grain, $P_e \pi {d_s}^2/4$, approaches or exceeds the weight of the grain, $(\rho_s - \rho)\frac{1}{6}\pi {d_s}^3 g$, with ρ_s denoting the sand density and g denoting the gravitational acceleration. Therefore, the critical values of P_e and k_t increase linearly with d_s. Because k_t is proportional to U^2 for the same ϕ (equation (1)), U_{crit} is expected to increase linearly with $\sqrt{d_s}$. In the present study, the ratio of $\sqrt{d_s}$ for the two grain sizes was between 1.4 and 1.8, thus the ratio of U_{crit} was expected to be 1.6 ± 0.2. The corresponding ratio between the measured U_{crit} values (Figure 3) was $1.9 \pm 0.2(SD)$. The agreement within uncertainty between the measured U_{crit} ratio and the expected ratio further supports the turbulence model.

5 Conclusions

Turbulence has been recognized to play an important role in initiating sediment motion. In a vegetated channel, the generation of turbulence in the wakes of vegetation elements exceeds that associated with bed-shear, such that previous bare-bed sediment-transport models based on bed shear stress alone do not work. This study developed a model for the critical velocity for the onset of sediment transport (U_{crit}) based on a threshold of near-bed turbulent kinetic energy (k_t). The model was validated by laboratory experiments conducted in both bare channels and channels with sparse model vegetation. At the critical condition when sediment started to move, the measured k_t was roughly a constant for all vegetation densities and bare bed (Figure 4), indicating that k_t may be a universal metric that predicts sediment motion in both bare and obstructed channels. Further, the k_t model for U_{crit} unified both the bare-bed and vegetated channel measurements (Figure 5). Previous experimental data with natural vegetation and natural mud also agreed with the new model within uncertainty, suggesting that the model can be extended to predict U_{crit} in natural conditions.

Acknowledgments

The work was supported by NSF grant EAR 1414499. The data in this study is available in excel format upon request from the authors. The authors would like to thank John Trowbridge and other Woods Hole scientists for providing insightful comments.

References

Buffin-Bélanger, T., and A. G. Roy (2005), 1 min in the life of a river: selecting the optimal record length for the measurement of turbulence in fluvial boundary layers, *Geomorphology*, *68*(1), 77–94.

Celik, A. O., P. Diplas, C. L. Dancey, and M. Valyrakis (2010), Impulse and particle dislodgement under turbulent flow conditions, *Physics of Fluids (1994-present)*, *22*(4), 046,601.

Celik, A. O., P. Diplas, and C. L. Dancey (2013), Instantaneous turbulent forces and impulse on a rough bed: Implications for initiation of bed material movement, *Water Resources Research*, *49*(4), 2213–2227.

Cheng, N.-S., and H. T. Nguyen (2011), Hydraulic radius for evaluating resistance induced by simulated emergent vegetation in open-channel flows, *Journal of hydraulic engineer-*

ing, *137*(9), 995–1004.

Costanza, R., R. d'Arge, R. De Groot, S. Faber, M. Grasso, B. Hannon, K. Limburg, S. Naeem, R. V. O'neill, J. Paruelo, et al. (1997), The value of the world's ecosystem services and natural capital.

Crocker, J. C., and D. G. Grier (1996), Methods of digital video microscopy for colloidal studies, *Journal of colloid and interface science*, *179*(1), 298–310.

Danielsen, F., M. K. Sørensen, M. F. Olwig, V. Selvam, F. Parish, N. D. Burgess, T. Hiraishi, V. M. Karunagaran, M. S. Rasmussen, L. B. Hansen, et al. (2005), The asian tsunami: a protective role for coastal vegetation, *Science(Washington)*, *310*(5748), 643.

Diplas, P., C. L. Dancey, A. O. Celik, M. Valyrakis, K. Greer, and T. Akar (2008), The role of impulse on the initiation of particle movement under turbulent flow conditions, *Science*, *322*(5902), 717–720.

Furbish, D. J., P. K. Haff, J. C. Roseberry, and M. W. Schmeeckle (2012), A probabilistic description of the bed load sediment flux: 1. theory, *Journal of Geophysical Research: Earth Surface*, *117*(F3).

Heathershaw, A., and P. Thorne (1985), Sea-bed noises reveal role of turbulent bursting phenomenon in sediment transport by tidal currents, *Nature*, *316*, 339–342.

Hongwu, T., H. Wang, D. Liang, S. Lv, and L. Yan (2013), Incipient motion of sediment in the presence of emergent rigid vegetation, *Journal of Hydro-environment Research*, *7*(3), 202–208.

Houssais, M., C. P. Ortiz, D. J. Durian, and D. J. Jerolmack (2015), Onset of sediment transport is a continuous transition driven by fluid shear and granular creep, *Nature communications*, *6*.

Julien, P. Y. (2010), *Erosion and sedimentation*, Cambridge University Press.

Kremen, C. (2005), Managing ecosystem services: what do we need to know about their ecology?, *Ecology letters*, *8*(5), 468–479.

Kundu, P., I. Cohen, and H. Hu (2008), Fluid mechanics. 2004, *Elsevier Academic Press, San Diego). Two-and three-dimensional self-sustained flow oscillations*, *307*, 471–476.

Liu, C., and H. Nepf (2016), Sediment deposition within and around a finite patch of model vegetation over a range of channel velocity, *Water Resources Research*, *52*(1), 600–612.

Marani, M., A. d'Alpaos, S. Lanzoni, and M. Santalucia (2011), Understanding and predicting wave erosion of marsh edges, *Geophysical Research Letters*, *38*(21).

Micheli, E., and J. Kirchner (2002), Effects of wet meadow riparian vegetation on stream-bank erosion. 2. measurements of vegetated bank strength and consequences for failure mechanics, *Earth Surface Processes and Landforms*, *27*(7), 687–697.

Nelson, J. M., R. L. Shreve, S. R. McLean, and T. G. Drake (1995), Role of near-bed turbulence structure in bed load transport and bed form mechanics, *Water Resources Research*, *31*(8), 2071–2086.

Nepf, H. M. (2012a), Hydrodynamics of vegetated channels, *Journal of Hydraulic Research*, *50*(3), 262–279.

Nepf, H. M. (2012b), Flow and transport in regions with aquatic vegetation, *Annual Review of Fluid Mechanics*, *44*, 123–142.

Nezu, I., H. Nakagawa, and G. H. Jirka (1994), Turbulence in open-channel flows, *Journal of Hydraulic Engineering*, *120*(10), 1235–1237.

Ricardo, A. M., K. Koll, M. J. Franca, A. J. Schleiss, and R. M. Ferreira (2014), The terms of turbulent kinetic energy budget within random arrays of emergent cylinders, *Water Resources Research*, *50*(5), 4131–4148.

Shields, A. (1936), Application of similarity principles and turbulence research to bed-load movement, *Tech. rep.*, Soil Conservation Service.

Smart, G., and H. Habersack (2007), Pressure fluctuations and gravel entrainment in rivers, *Journal of Hydraulic Research*, *45*(5), 661–673.

Stapleton, K., and D. Huntley (1995), Seabed stress determinations using the inertial dissipation method and the turbulent kinetic energy method, *Earth Surface Processes and Landforms*, *20*(9), 807–815.

Stoesser, T., S. Kim, and P. Diplas (2010), Turbulent flow through idealized emergent vegetation, *Journal of hydraulic engineering*, *136*(12), 1003–1017.

Tanino, Y., and H. Nepf (2007), Experimental investigation of lateral dispersion in aquatic canopies, in *PROCEEDINGS OF THE CONGRESS-INTERNATIONAL ASSOCIATION FOR HYDRAULIC RESEARCH*, vol. 32, p. 152.

Tanino, Y., and H. M. Nepf (2008a), Lateral dispersion in random cylinder arrays at high reynolds number, *Journal of Fluid Mechanics*, *600*, 339–371.

Tanino, Y., and H. M. Nepf (2008b), Laboratory investigation of mean drag in a random array of rigid, emergent cylinders, *Journal of Hydraulic Engineering*, *134*(1), 34–41.

Taylor, J. (1997), *Introduction to error analysis, the study of uncertainties in physical measurements*, vol. 1.

Tinoco, R., and G. Coco (2014), Observations of the effect of emergent vegetation on sediment resuspension under unidirectional currents and waves, *Earth Surface Dynamics*, *2*(1), 83.

Vowinckel, B., R. Jain, T. Kempe, and J. Fröhlich (2016), Entrainment of single particles in a turbulent open-channel flow: a numerical study, *Journal of Hydraulic Research*, *54*(2), 158–171.

Widdows, J., N. D. Pope, and M. D. Brinsley (2008), Effect of spartina anglica stems on near-bed hydrodynamics, sediment erodability and morphological changes on an intertidal mudflat, *Marine Ecology Progress Series*, *362*, 45–57.

Wilcock, P. R. (1996), Estimating local bed shear stress from velocity observations, *Water Resources Research*, *32*(11), 3361–3366.

Wong, M., G. Parker, P. DeVries, T. M. Brown, and S. J. Burges (2007), Experiments on dispersion of tracer stones under lower-regime plane-bed equilibrium bed load transport, *Water Resources Research*, *43*(3).

Yager, E., and M. Schmeeckle (2013), The influence of vegetation on turbulence and bed load transport, *Journal of Geophysical Research: Earth Surface*, *118*(3), 1585–1601.

Yang, J. Q., F. Kerger, and H. M. Nepf (2015), Estimation of the bed shear stress in vegetated and bare channels with smooth beds, *Water Resources Research*, *51*(5), 3647–3663.

Zanke, U. (2003), On the influence of turbulence on the initiation of sediment motion, *International Journal of Sediment Research*, *18*(1), 17–31.